

Lattice instability, anharmonicity and Raman spectra of BaO under high pressure: A first principles study

K. Lavanya,^{†,‡} N. Yedukondalu,^{*,¶} S. C. Rakesh Roshan,^{§,||} Shweta D. Dabhi,[⊥]
Suresh Sripada,[#] M.Sainath,^{*,@} Lars Ehm,[¶] and John B. Parise[¶]

[†]*Jawaharlal Nehru Technological University (JNTU), Hyderabad, 500085, Telangana, India.*

[‡]*Telangana Social Welfare Residential Degree College for Women (TSWRDC-W), Nizamabad, 503002, Telangana, India.*

[¶]*Department of Geosciences, State University of New York, Stony Brook, New York 11794-2100, USA*

[§]*Rajiv Gandhi University of Knowledge Technologies, Basar, Telangana-504107, India*

^{||}*Department of Physics, National Institute of Technology-Warangal, Telangana, India*

[⊥]*Department of Physical Sciences, P D Patel Institute of Applied Sciences, Charotar University of Science and Technology, CHARUSAT Campus, Changa, 388421, Gujarat, India*

[#]*Department of Physics, JNTUHCEJ, 505501 Karimnagar, Telangana, India*

[@]*Department of Physics, IcfaiTech, IFHE, Hyderabad 501203, Telangana, India.*

E-mail: nykondalu@gmail.com; sai1968@gmail.com

Abstract

Alkaline-earth metal oxides, in particular MgO and CaO dominate Earth's lower mantle, therefore, exploring high pressure behavior of this class of compounds is of significant geophysical research interest. Among the alkaline-earth metal oxides, BaO exhibits rich polymorphism in the pressure range of 0-1.5 Mbar. Static enthalpy calculations revealed that BaO undergoes a pressure induced structural phase transition from NaCl-type (B1) \rightarrow NiAs-type (B8) \rightarrow distorted CsCl-type (d-B2) \rightarrow CsCl-type (B2) at 5.1, 19.5, 120 GPa respectively. B1 \rightarrow B8 & B8 \rightarrow d-B2 transitions are found to be first order in nature whereas d-B2 \rightarrow B2 is a second order or weak first order phase transition with displacive nature. Interestingly, d-B2 phase shows stability over a wide pressure range of \sim 19.5-113 GPa. Mechanical and dynamical stabilities of ambient and high pressure phases are demonstrated through the computed second order elastic constants and phonon dispersion curves, respectively. Under high pressure, significant phonon softening and soft phonon mode along M-direction are observed for B8, d-B2 and B2 phases, respectively. Pressure dependent Raman spectra suggests a phase transition from d-B2 to Raman inactive phase under high pressure. Overall, the present study provides a comprehensive understanding of lattice dynamics and underlying mechanisms behind pressure induced structural phase transitions in BaO.

Keywords:- High pressure, Phase transitions, Elastic constants, Lattice dynamics, Phonon softening, Lattice instability, Anharmonicity, Earth's interior

Introduction

Alkaline-earth metal oxides, MO (M = Mg, Ca, Sr, Ba) have gained a considerable attention due to their technological applications in diverse fields,¹⁻⁵ ranging from catalysis⁶⁻⁸ to electrode coating⁹ and interfaces.¹⁰ These metal oxides are suitable candidates for CO₂ sorbent applications due to their high absorption capacity at moderate temperatures.³ Moreover, these mono-oxides are prime candidates for the Earth's interior, especially light metal oxides

such as MgO and CaO are abundant in the Earth’s lower mantle, in which the pressure varies from 24 to 136 GPa from top of the upper mantle to the lower mantle.^{11–15} Therefore, exploring high pressure and/or temperature behavior of these metal oxides provides an insight on the deep interior of the Earth. These metal oxides crystallize in the rocksalt NaCl-type (B1) structure with space group $Fm\bar{3}m$ at ambient conditions. Upon compression, these metal oxides usually undergo a body centred cubic CsCl-type (B2) structure and it is well established for MgO, CaO and SrO. Amongst all these compounds, BaO has interesting structural properties and it exhibits a rich polymorphism in the pressure range of 0-1.5 Mbar over the remaining alkaline earth oxides, CaO,^{16–24} SrO.^{16–19,25–29} Therefore, understanding the high pressure structural and lattice dynamical behavior of BaO is crucial as this can be a possible candidate of the Earth’s mantle.¹² Several high pressure X-ray diffraction (HP-XRD) measurements^{23,29–35} and theoretical studies using first principles calculations were focused on exploring the structural phase transitions,^{18,21,25,27,36–39} metallization,^{20,40–46} elastic properties,^{47–50} thermodynamic stability^{25,51,52} of MO (M = Mg, Ca, Sr, Ba) compounds under high pressure. Similarly, efforts have been put forward by the researchers to explore the phase diagram of BaO under high pressure from both experimental and theoretical perspective. A HP-XRD study³⁰ revealed that BaO undergoes a structural transition from B1 to distorted B2 (d-B2) at 9.2 GPa and remains in the same structure till 29 GPa. Energy dispersive X-ray diffraction study³¹ disclosed that BaO transforms from B1 to an intermediate hexagonal NiAs-type (B8) structure at around 10 GPa, later to a tetragonal PH₄I-type (d-B2) structure with pseudo 8-fold coordination at around 15 GPa and this phase approaches to B2 structure with increasing pressure above 1 Mbar. First principles studies^{17,53,54} reported that BaO transforms from B1 to B8 phase at 11.3 GPa,⁵³ 5 GPa,¹⁷ 4.3 GPa⁵⁴ then to d-B2 from B8 at 21.5 GPa,⁵³ 13 GPa,¹⁷ 23.2 GPa,⁵⁴ upon further compression, the d-B2 phase transforms to B2 phase at 62 GPa,⁵³ 50 GPa,¹⁷ 108 GPa.⁵⁴ Pandey et al⁴⁹ and Jog et al⁵⁵ suggested a direct B1 to B2 phase transition at 100 and 86 GPa, respectively without any intermediate high pressure phases.

On the other hand, lattice dynamics of B1 phase is well studied at ambient as well as at high pressure using first principles calculations^{16,51,56,57} and inelastic neutron scattering technique.⁵⁸ However, very limited studies⁵² are available exploring lattice dynamics of high pressure phases, underlying mechanisms behind the observed structural phase transitions and spectroscopic properties under high pressure in BaO. Therefore, in the present study, we have systematically investigated the structural phase transitions, lattice dynamics of different polymorphs and Raman spectra of B8 and d-B2 phases of BaO under high pressure.

Computational details

All the first principles calculations were carried out using projected augmented wave (PAW) method as implemented in Vienna ab-initio simulation package (VASP).⁵⁹ Electron-electron interactions are treated within generalized gradient approximation (GGA) with Perdew–Burke–Ernzerhof (PBE) functional while PAW pseudopotentials are used to capture the electron-ion interactions. The plane wave basis orbitals $5s^25p^66s^2$ for Ba (Ba_sv_GW) and $2s^22p^4$ for O (O_GW) are used as valence electrons. Plane wave cutoff energy and k-spacing are tested against the total energy to ensure the convergence. The plane wave cutoff energy was set to 600 eV and a k-spacing of $2\pi \times 0.024 \text{ \AA}^{-1}$ with Γ -centered Monkhorst-Pack scheme to compute structural and mechanical properties at ambient as well as at high pressure. To compute phonon dispersion curves, forces are calculated using finite displacement method for ambient and high pressure phases and then force constants are extracted and then post-processed by using phonopy package.⁶⁰ Pressure dependent Raman spectra is calculated using norm conserving pseudo potentials within linear response approach as implemented in CASTEP package.⁶¹ Crystal structures are visualized and analyzed using the VESTA software.⁶² To include anharmonic effects, we also have calculated the finite temperature lattice dynamics for B2 phase of BaO using ab-initio molecular dynamics (AIMD) simulations and then post-processed using temperature dependent effective potential method (TDEP).⁶³

Results and Discussion

Crystal structure and pressure-induced structural phase transitions

As shown in Figure 1a, BaO crystallizes in the face centred cubic (SG: $Fm\bar{3}m$) rocksalt NaCl-type (B1) structure with 6-fold coordination and having $Z = 4$ formula units (f.u.) per unit cell at ambient conditions.³¹ High pressure X-ray diffraction measurements^{30,31,64} revealed that BaO exhibits rich polymorphism under high pressure. BaO undergoes to a high pressure NiAs-type (B8) structure (SG: $P6_3/mmc$) from B1 phase at 9.2 GPa without changing the coordination number (CN) by having $Z = 2$ f.u. per primitive cell. The crystal structure of B8 phase is an hexagonal analog of the B1 structure. Later, the B8 phase transforms to PH₄-type distorted CsCl-type (d-B2) at 14.0 GPa,³⁰ 18 GPa³⁰ with pseudo 8-fold coordination (SG: $P4/nmm$) with $Z = 2$ f.u. per primitive cell, and then to a 8-fold coordinated CsCl-type (B2) structure (SG: $Pm\bar{3}m$) with $Z = 1$ f.u. per primitive cell upon further compression *i.e.*, above 1 Mbar pressure (see Figure 1 and Table 1).^{30,31,64} The crystal structure of d-B2 phase is analogous to PbO-type structure without a lone-pair at Ba atom having two in-equivalent bond lengths as shown in Figure 1c. To get further insights on the observed structural phase transitions and their sequence, as a first step, we have tested with various DFT functionals such as LDA, PBE, PW91 and SCAN to reproduce the B1 to B8 transition pressure (see Figure S1). The transition pressure obtained using PBE, PW91 and SCAN functionals are consistent with each other while LDA poorly describe the phase stability between B1 and B8 phases. Later, we carried out static enthalpy calculations with PBE functional for the polymorphic phases of BaO and plotted enthalpy difference with respect to B2 phase as a function of pressure as shown in Figure 2a. The obtained phase transition sequence is B1 \rightarrow B8 \rightarrow d-B2 \rightarrow B2 and the corresponding transition pressures 5.1, 19.5, 120 GPa are in good agreement with the HP-XRD measurements^{30,31} as well as with previous first principles calculations.^{52,53} Moreover, TII-type (B33) phase is found to be meta-stable for CaO⁶⁵ and we also have included this B33 phase in the phase diagram

of BaO to verify its relative phase stability w.r.t high pressure phases of BaO and then we found that the B33 phase is also meta-stable for BaO over the maximum studied pressure range (see Figure 2a). As presented in Figure 2b, the enthalpy difference between d-B2 and B2 phases is continuously decreasing with increasing pressure and they become iso-enthalpic at around 120 GPa. As shown in Figure 2c, the calculated lattice constants for the ambient and high pressure phases are monotonically decreasing with pressure. The lattice constant 'c' of d-B2 phase becomes lattice constant 'a' for B2 phase ($c_{d-B2} = a_{B2}$). The detailed transition mechanism for d-B2 to B2 transition is explained through elastic constants in the following section. As shown in Figure 2d, the calculated volume decreases monotonically with pressure. We observe a volume collapse during the phase transition from B1 \rightarrow B8 is $\sim 3.65\%$ at 5.1 GPa and it is $\sim 6.4\%$ at 19.5 GPa for the transition B8 \rightarrow d-B2. The obtained volume reduction is consistent with high pressure X-diffraction measurements and previous first principles calculations as presented in Table 2. This clearly demonstrates that B1 to B8 & B8 to d-B2 transitions are first order in nature, while d-B2 to B2 transition is a second order or weak first order in nature due to continuous change in volume during the phase transition (see Figure 2d). We then calculated the equilibrium bulk modulus (B_0) and its pressure derivative (B_0') by fitting the obtained pressure-volume (P-V) data to 3rd order Birch-Murnaghan equation of state,⁶⁶ B_0 measures the ability of a material to resist changes in volume under hydrostatic expansion or compression. The calculated B_0 value is found to be 71.4 GPa for the ambient B1 phase, which is in good agreement with previous first principles calculations.⁶⁷ The obtained relatively low B_0 values 68.8 GPa for B8 and 51.8 for d-B2 intermediate phases suggest the soft nature of these phases over ambient B1 (71.4 GPa) and a high B_0 value 92.4 GPa for high pressure B2 phase disclose that B2 phase is harder than B1 phase (see Table 3).

In addition, the calculated in-equivalent bond lengths are plotted as a function of pressure and the same are presented in Figure 2e. The in-equivalent bond lengths of d-B2 phase are found to converge to become a single bond length for B2 phase above 120 GPa. In addition,

in the d-B2 phase, the Ba atoms are located at $(0.5, 0.0, 0.5+\Delta)$ and $(0.0, 0.5, 0.5-\Delta)$, where Δ is the atomic position parameter, Δ in combination axial ratio (c/a) provides a useful information on d-B2 \rightarrow B2 transition. If $\Delta = 0$ & $c/a = 1/\sqrt{2} = 0.7071$, then the structure is of undistorted B2 phase.³¹ To confirm this, we have calculated c/a ratio and Δ as a function of pressure for d-B2 phase. As shown in Figure 2f, both c/a ratio and Δ are decreasing with pressure and then approaches to $\Delta = 0$ & $c/a = 0.7071$ around 120 GPa. The continuous volume change at the transition pressure, variation in the fractional coordinate of Ba atom along c-direction (see Figure S2), $c/a = 0.7071$ and $\Delta = 0$ values clearly demonstrate that d-B2 to B2 transition to be a displacive transition under pressure. Displacive nature of z_{Ba} with pressure suggests phonon softening in d-B2 phase as function of pressure. Further to explore the microscopic origin of the continuous phase transition in BaO, pressure dependent elastic constants, lattice dynamics and Raman spectra are calculated and analyzed them in detail in the following sections.

Elastic constants under high pressure

To get deeper insight on the structural phase transition(s) and verify mechanical stability of the BaO polymorphs, we have calculated second order elastic constants (C_{ij}) as a function of pressure for all the four B1, B8, d-B2 and B2 phases. The cubic ($Fm\bar{3}m$, $Pm\bar{3}m$), hexagonal ($P6_3/mmc$) and tetragonal ($P4/nmm$) crystal symmetries possess 3, 5 and 6 independent elastic constants.

When a finite hydrostatic pressure is applied to a crystal system, the Born stability criteria⁶⁸ at ambient conditions must be revised with modified elastic constants at a given hydrostatic pressure conditions. According to Sinko and Smirnov the modified elastic constants at a given pressure (P) are $\tilde{C}_{ii} = C_{ii} - P$, (for $i = 1-6$) and $\tilde{C}_{1j} = C_{1j} + P$ (for $j = 2-3$) for cubic and hexagonal/tetragonal systems. Therefore, the modified Born stability criteria under hydrostatic pressure for cubic (equation 1) and hexagonal/tetragonal (equation 2) are

given as follows:

$$C_{11} - C_{12} - 2P > 0, \quad C_{11} + 2C_{12} + P > 0, \quad C_{44} - P > 0 \quad (1)$$

$$\begin{aligned} C_{11} - C_{12} - 2P > 0, \\ P^2 + P(C_{11} + C_{12} + 4C_{13}) + 2C_{13}^2 - C_{33}(C_{11} + C_{12}) > 0, \\ C_{44} - P > 0, \quad C_{66} - P > 0 \end{aligned} \quad (2)$$

The calculated pressure dependent C_{ij} for B1, B8, d-B2 and B2 phases satisfy the necessary and sufficient conditions for the revised Born stability criteria under hydrostatic pressure indicating that the polymorphs are mechanically stable at the corresponding pressures. We shed more light on understanding lattice transformation from d-B2 to B2 phase through the computed pressure dependent elastic constants of d-B2 and B2 phases. The relationships between lattice constants of d-B2 and B2 phases at the phase transition are given as follows: $(a=b)_{d-B2} = \sqrt{2}c_{d-B2}$ and $c_{d-B2} = a_{B2}$ (see Figure 3a), thus, results in merging of the following elastic constants of d-B2 to B2 phase under pressure are as depicted in Figure 3 as given below: $C_{33}^{d-B2} \rightarrow C_{11}^{B2}$, $C_{44}^{d-B2} \rightarrow C_{44}^{B2}$ and $C_{13}^{d-B2} \rightarrow C_{12}^{B2}$, which corroborates with pressure dependent structural and bond parameters at the d-B2 \rightarrow B2 transition.

Lattice dynamics and Raman spectra under high pressure

To compliment the structural stability obtained from total energy calculations and verify dynamical stability of the ambient and high pressure phases of BaO, we calculated phonon dispersion curves including LO-TO splitting at 0 and 9 GPa for B1 phase (see Figure 4a & b) at 9 GPa and 20 GPa for B8 phase (see Figure 4c & d), at 30, 60, 90 and 120 GPa for d-B2 phase (see Figure 5) and finally at 100, 110, 120 and 140 GPa for B2 phase (see Figure 6). As shown in Figure 4a & b, B1 and B8 phases are dynamically stable at 0, 9 GPa and 9, 20 GPa

respectively. The phonon dispersion curves of B1 phase show large LO-TO splitting ($\sim 312.3 \text{ cm}^{-1}$) along Γ -direction with two degenerate TO and one LO modes and this large LO-TO splitting causes a fall of low lying optical (LLO) phonon modes into acoustic mode region, which can increase overlap between acoustic and LLO phonon modes there by enhancing the scattering phase space and eventually this leads to lower the lattice thermal conductivity in B1 phase at ambient conditions.⁶⁹ However, the LO-TO splitting decreases under pressure (see Figure 4a & b) for B1 phase. Moreover, the optical phonon modes are hardening with pressure while phonon softening is observed for acoustic phonon modes along X-direction in B1 phase and along M and K- Γ directions in B8 phase. Phonon softening is observed along X-direction for B1 phase previously,⁵² which actually drives the transition from B1 \rightarrow B8 phase in BaO under pressure. In addition, the B1 and B8 phases are dynamically stable above the transition pressures, which are in consistent with the first order nature of the structural phase transitions, B1 \rightarrow B8 & B8 \rightarrow d-B2. The d-B2 phase is found to be dynamically stable over a wide pressure range of ~ 20 -120 GPa (see Figure 5) for BaO in contrast to the light alkaline-earth metal oxides, MgO, CaO and SrO. The calculated phonon dispersion curves show a significant phonon softening at 120 GPa along Z- Γ and 'A' high symmetry directions as depicted in Figure 5d. On the other hand, the calculated phonon dispersion curves for B2 phase at 100 and 110 GPa show soft phonon mode along M high symmetry point, which clearly indicates that B2 is unstable below 110 GPa pressure. In addition, we could also observe a significant phonon softening of TO and LO modes of B2 phase at 140 GPa (see Figure 6d) compared to 120 GPa (see Figure 6b), which indicates that B2 phase becomes dynamically unstable and it may undergo a structural phase transition upon further compression above 150 GPa.

The cubic ambient B1 and high pressure B2 phases of BaO are Raman inactive, and they have only one IR active (T_{1u}) mode. However, the intermediate high pressure B8 and d-B2 phases are Raman active, and are thoroughly analyzed (see Figure 7). This result is in very good agreement with the Raman spectroscopic measurements,⁷⁰ which show that BaO

is Raman inactive until 10 GPa (B1 phase) and above 11 GPa it becomes Raman active (B8), where one Raman active E_{2g} mode is observed and this Raman mode shows blue-shift with increasing pressure. Later, significant changes are observed in the Raman spectra at around 14 GPa and it indicates a transition from B8 to d-B2 phase. The similar trends are observed in the present work with deviations in the transition pressures which might be due to Raman measurements were carried out at 300 K, while the calculations are performed at 0 K. Since, B8 and d-B2 phases crystallize in $P6_3/mmc$ and $P4/nmm$ space groups, respectively and they consist of four atoms per primitive cell, the symmetry decomposition of group theory predicts 12 vibrational modes along Γ for both of these phases, which are given as follows:

$$\Gamma_{12}^{B8} = 2E_{2g} \oplus B_{2g} \oplus 4E_{1u} \oplus 2E_{2u} \oplus 2A_{2u} \oplus B_{1u}$$

Among the 12 vibrational modes of B8 phase, only E_{2g} is Raman active mode which is consistent with high pressure Raman measurements,⁷⁰ E_{1u} , E_{2u} , A_{2u} and B_{1u} are IR active modes but B_{2g} is neither Raman nor IR active (silent) mode; where E_{1u} , E_{2u} and E_{2g} are doubly degenerate modes. Variation of E_{2g} mode as a function of pressure is shown in Figure 7a, which is mainly due to in-plane vibrational motion of Ba atom and its intensity decreases with pressure.

$$\Gamma_{12}^{d-B2} = 4E_g \oplus B_{2g} \oplus A_{1g} \oplus 4E_u \oplus 2A_{2u}$$

On the other hand, for Litharge PbO-type d-B2 phase, the zone-center Raman active modes B_{2g} , A_{1g} and E_g are polarized along c- and a/b-axis, respectively. E_u and A_{2u} are IR active modes; where E_u and E_g modes are doubly degenerate. Pressure dependence of vibrational frequency modes are presented in Figure 7d. For each vibrational mode, frequency increases with pressure except for A_{1g} mode. When the pressure is applied, the interatomic distance becomes smaller and hence interaction between neighboring atoms becomes stronger. Therefore, usually, the vibrational modes increase with pressure as shown in Figure 7b & d except for A_{1g} mode. As E_g mode is in plane vibrational mode, the vibrational fre-

quency/wavenumber increases as the interaction of atoms becomes stronger. As shown in Figure 2f; c/a ratio decreases with increasing pressure. Due to the out-of-plane vibrations of heavier Ba atoms in A_{1g} mode (Figure 7c), the decrease in the wavenumber of Raman-shift is observed with pressure. The red-shift of the A_{1g} mode with pressure shows a negative pressure coefficient and it might be responsible for introducing dynamical instability at higher pressure in the d-B2 phase. In contrast, this mode was tentatively assigned as E_g mode due to in-plane vibration of Ba atoms in the HP-Raman study.⁷⁰ However, we thoroughly analyzed and assigned it as A_{1g} mode rather than E_g mode, which actually shows phonon softening with pressure which is associated with displacive nature of Ba atoms along c -axis. The Intensity of four Raman active modes (E_g , B_{2g} and A_{1g}) are gradually diminishing with pressure (Figure 7b) for d-B2 phase, this strongly suggests that high pressure phase might be Raman inactive. Finally, the high pressure B2 phase can be stabilized above 113 GPa (see Figure 7e) which is consistent with the observations from the HP-XRD measurements.³¹

As shown in Figure S3 & 6, the calculated room temperature phonon dispersion curves in combination with AIMD and TDEP disclose that B2 phase is dynamically unstable at 80 GPa and 300 K whereas it becomes dynamically stable at 100 GPa and 300 K, while harmonic lattice dynamical calculations show that B2 phase is dynamically unstable below ~ 113 GPa. This clearly shows the importance of anharmonicity to determine the stability of B2 phase above 85 GPa and this is in good accord with the HP-XRD diffraction measurements.³¹

Conclusions

To summarize, we have systematically investigated the polymorphism of BaO under hydrostatic compression using first principles calculations based on density functional theory. We found that BaO undergoes series of pressure-induced structural phase transitions from B1 \rightarrow B8 \rightarrow d-B2 \rightarrow B2 and the corresponding transition pressures are 5.1 , 19.5, 120 GPa respectively. The obtained structural phase transition sequence and transition pressures are

consistent with HP-XRD measurements and previous first principles calculations. TII-type (B33) phase is found to be metastable for BaO over the studied pressure range. The d-B2 phase exhibits stability over a wide pressure range ~ 19.5 -113 GPa in contrast to light alkaline-earth metal oxides. The transitions from B1 \rightarrow B8 and B8 \rightarrow d-B2 are first order in nature with a volume collapse of ~ 3.65 and 6.4 %, respectively while d-B2 \rightarrow B2 is a second order or weak first order phase transition with displacive nature. Mechanical stability has been established for ambient and high pressure phases of BaO through computed elastic constants. The pressure dependent elastic constants provide an insight on lattice transformation from d-B2 to B2 phase. The calculated phonon dispersion curves indicate the dynamical stability of BaO polymorphs and a significant phonon softening is observed for B8 and d-B2 phases at high pressures and also a soft phonon mode (along M-direction) in B2 phase explained its dynamical instability below 110 GPa. Finally, gradual diminishing of Raman active modes of d-B2 phase under pressure suggests that high pressure phase could be a Raman inactive. Overall, the present study provides an in depth understanding of structural phase transitions in BaO under high pressure and further exploration of high pressure behavior of light alkaline-earth oxides (MgO, CaO and SrO) have important implications on composition of the Earth's lower mantle.

Acknowledgments

LV and NYK contributed equally to this manuscript. NYK would like to thank Science and Engineering Research Board and Indo-US Scientific Technology Forum for providing financial support through SERB Indo-US postdoctoral fellowship and Institute for Advanced Computational Science, Stony Brook University for providing computational resources (Seawulf cluster). SCRR would like thank RGUKT Basar for providing computational facilities.

References

- (1) Cho, J.; Kim, R.; Lee, K.-W.; Yeom, G.-Y.; Kim, J.-Y.; Park, J.-W. Effect of CaO addition on the firing voltage of MgO films in AC plasma display panels. *Thin Solid Films* **1999**, *350*, 173–177.
- (2) Speier, W.; Szot, K. Physics and chemistry at oxide surfaces. By Claudine Noguera, Cambridge university press, Cambridge 1996, xv, 223 pp., hardcover, £40.00, ISBN 0-52147214-8. *Advanced Materials* **1997**, *9*, 1192–1193.
- (3) Duan, Y.; Sorescu, D. C. CO₂ capture properties of alkaline earth metal oxides and hydroxides: A combined density functional theory and lattice phonon dynamics study. *The Journal of Chemical Physics* **2010**, *133*, 074508.
- (4) Medeiros, S. K.; Albuquerque, E. L.; Maia, F. F.; de Sousa, J. S.; Caetano, E. W. S.; Freire, V. N. CaO first-principles electronic properties and MOS device simulation. *Journal of Physics D: Applied Physics* **2007**, *40*, 1655–1658.
- (5) Zannotti, M.; Wood, C. J.; Summers, G. H.; Stevens, L. A.; Hall, M. R.; Snape, C. E.; Giovanetti, R.; Gibson, E. A. Ni Mg Mixed Metal Oxides for p-Type Dye-Sensitized Solar Cells. *ACS Applied Materials & Interfaces* **2015**, *7*, 24556–24565.
- (6) Prinetto, F.; Ghiotti, G.; Nova, I.; Castoldi, L.; Lietti, L.; Tronconi, E.; Forzatti, P. In situ FT-IR and reactivity study of NO_x storage over Pt–Ba/Al₂O₃ catalysts. *Phys. Chem. Chem. Phys.* **2003**, *5*, 4428–4434.
- (7) Choudhary, V.; Rajput, A.; Mamman, A. NiO-Alkaline Earth Oxide Catalysts for Oxidative Methane-to-Syngas Conversion: Influence of Alkaline Earth Oxide on the Surface Properties and Temperature-Programmed Reduction/Reaction by H₂ and Methane. *Journal of Catalysis* **1998**, *178*, 576–585.

- (8) Au, C.; Chen, K.; Ng, C. The modification of Gd_2O_3 with BaO for the oxidative coupling of methane reactions. *Applied Catalysis A: General* **1998**, *170*, 81–92.
- (9) Mishra, K. C.; Garner, R.; Schmidt, P. C. Model of work function of tungsten cathodes with barium oxide coating. *Journal of Applied Physics* **2004**, *95*, 3069–3074.
- (10) McKee, R. A.; Walker, F. J.; Chisholm, M. F. Physical Structure and Inversion Charge at a Semiconductor Interface with a Crystalline Oxide. *Science* **2001**, *293*, 468–471.
- (11) Chen, G.; Liebermann, R. C.; Weidner, D. J. Elasticity of Single-Crystal MgO to 8 Gigapascals and 1600 Kelvin. *Science* **1998**, *280*, 1913–1916.
- (12) Margrave, J. High pressure research, applications in geophysics. *Physics of the Earth and Planetary Interiors* **1979**, *20*, 74.
- (13) Bovolo, C. I. The physical and chemical composition of the lower mantle. *Philosophical Transactions of the Royal Society A: Mathematical, Physical and Engineering Sciences* **2005**, *363*, 2811–2836.
- (14) Anderson, D. L. *Theory of the Earth*; Blackwell scientific publications, 1989.
- (15) McDonough, W.; Sun, S. The composition of the Earth. *Chemical Geology* **1995**, *120*, 223–253.
- (16) Aguado, A.; Bernasconi, L.; Madden, P. A. Interionic potentials from ab initio molecular dynamics: The alkaline earth oxides CaO, SrO, and BaO. *The Journal of Chemical Physics* **2003**, *118*, 5704–5717.
- (17) Alfredsson, M.; Brodholt, J. P.; Wilson, P. B.; Price, G. D.; Corà, F.; Calleja, M.; Bruin, R.; Blanshard, L. J.; Tyer, R. P. Structural and magnetic phase transitions in simple oxides using hybrid functionals. *Molecular Simulation* **2005**, *31*, 367–377.

- (18) Cinthia, A. J.; Priyanga, G. S.; Rajeswarapalanichamy, R.; Iyakutti, K. Structural, electronic and mechanical properties of alkaline earth metal oxides MO (M=Be, Mg, Ca, Sr, Ba). *Journal of Physics and Chemistry of Solids* **2015**, *79*, 23–42.
- (19) Pozhivatenko, V. Ionic Character, Phase Transitions, and Metallization in Alkaline-Earth Metal Oxides and Chalcogenides under Pressure. *Ukrainian Journal of Physics* **2020**, *65*, 1022.
- (20) Kunduru, L.; Yedukondalu, N.; Roshan, S. R.; Sripada, S.; Sainath, M. Structural phase transition and electronic structure of binary CaO and SrO under high pressure. *Materials Today: Proceedings* **2021**,
- (21) Kürkçü, C.; Merdan, Z.; Yamçıgıer, Ç. Structural phase transition and electronic properties of CaO under high pressure. *Materials Research Express* **2018**, *5*, 125903.
- (22) Kholiya, K.; Verma, S.; Pandey, K.; Gupta, B. High-pressure behavior of calcium chalcogenides. *Physica B: Condensed Matter* **2010**, *405*, 2683–2686.
- (23) Jeanloz, R.; Ahrens, T. J.; Mao, H. K.; Bell, P. M. B1-B2 Transition in Calcium Oxide from Shock-Wave and Diamond-Cell Experiments. *Science* **1979**, *206*, 829–830.
- (24) Bhardwaj, P.; Singh, S. Role of temperature in the numerical analysis of CaO under high pressure. *Open Chemistry* **2010**, *8*, 126–133.
- (25) Hou, X.-Y.; Tan, J.; Hu, C.-E.; Chen, X.-R.; Geng, H.-Y. Thermoelectric properties of strontium oxide under pressure: First-principles study. *Physics Letters A* **2021**, *390*, 127083.
- (26) Lukačević, I. High pressure lattice dynamics, dielectric and thermodynamic properties of SrO. *Physica B: Condensed Matter* **2011**, *406*, 3410–3416.
- (27) Salam, M. M. A. First principles study of structural, elastic and electronic structural properties of strontium chalcogenides. *Chinese Journal of Physics* **2019**, *57*, 418–434.

- (28) Souadkia, M.; Bennecer, B.; Kalarasse, F. Ab initio lattice dynamics and thermodynamic properties of SrO under pressure. *Journal of Physics and Chemistry of Solids* **2012**, *73*, 129–135.
- (29) Sato, Y.; Jeanloz, R. Phase transition in SrO. *Journal of Geophysical Research* **1981**, *86*, 11773.
- (30) Liu, L.-g.; Bassett, W. A. Effect of pressure on the crystal structure and the lattice parameters of BaO. *Journal of Geophysical Research (1896-1977)* **1972**, *77*, 4934–4937.
- (31) Weir, S. T.; Vohra, Y. K.; Ruoff, A. L. High-pressure phase transitions and the equations of state of BaS and BaO. *Physical Review B* **1986**, *33*, 4221–4226.
- (32) Rieder, K. H.; Weinstein, B. A.; Cardona, M.; Bilz, H. Measurement and Comparative Analysis of the Second-Order Raman Spectra of the Alkaline-Earth Oxides with a NaCl Structure. *Physical Review B* **1973**, *8*, 4780–4786.
- (33) Galtier, M.; Montaner, A.; Vidal, G. Phonons Optiques de CaO, SrO, BaO Au Centre de la Zone de Brillouin à 300 et 17K. *Journal of Physics and Chemistry of Solids* **1972**, *33*, 2295–2302.
- (34) Miyanishi, K.; Tange, Y.; Ozaki, N.; Kimura, T.; Sano, T.; Sakawa, Y.; Tsuchiya, T.; Kodama, R. Laser-shock compression of magnesium oxide in the warm-dense-matter regime. *Physical Review E* **2015**, *92*.
- (35) Root, S.; Shulenburger, L.; Lemke, R. W.; Dolan, D. H.; Mattsson, T. R.; Desjarlais, M. P. Shock Response and Phase Transitions of MgO at Planetary Impact Conditions. *Physical Review Letters* **2015**, *115*.
- (36) Duan, Y.; Qin, L.; Tang, G.; Shi, L. First-principles study of ground- and metastable-state properties of XO (X = Be, Mg, Ca, Sr, Ba, Zn and Cd). *The European Physical Journal B* **2008**, *66*, 201–209.

- (37) Rajput, K.; Roy, D. R. Structure, stability, electronic and thermoelectric properties of strontium chalcogenides. *Physica E: Low-dimensional Systems and Nanostructures* **2020**, *119*, 113965.
- (38) Bouchet, J.; Bottin, F.; Recoules, V.; Remus, F.; Morard, G.; Bolis, R. M.; Benuzzi-Mounaix, A. Ab initio calculations of the B1-B2 phase transition in MgO. *Physical Review B* **2019**, *99*.
- (39) Yu, J.; Zhang, M.; Zhang, Z.; Wang, S.; Wu, Y. Hybrid-functional calculations of electronic structure and phase stability of MO (M = Zn, Cd, Be, Mg, Ca, Sr, Ba) and related ternary alloy $MxZn_{1-x}O$. *RSC Advances* **2019**, *9*, 8507–8514.
- (40) Ghebouli, B.; Ghebouli, M.; Fatmi, M.; Benkerri, M. First-principles calculations of structural, elastic, electronic and optical properties of XO (X=Ca, Sr and Ba) compounds under pressure effect. *Materials Science in Semiconductor Processing* **2010**, *13*, 92–101.
- (41) Baltache, H.; Khenata, R.; Sahnoun, M.; Driz, M.; Abbar, B.; Bouhafis, B. Full potential calculation of structural, electronic and elastic properties of alkaline earth oxides MgO, CaO and SrO. *Physica B: Condensed Matter* **2004**, *344*, 334–342.
- (42) Baumeier, B.; Krüger, P.; Pollmann, J. Bulk and surface electronic structures of alkaline-earth metal oxides: Bound surface and image-potential states from first principles. *Physical Review B* **2007**, *76*.
- (43) Beiranvand, R. Hybrid exchange–correlation energy functionals for accurate prediction of the electronic and optical properties of alkaline-earth metal oxides. *Materials Science in Semiconductor Processing* **2021**, *135*, 106092.
- (44) Sobolev, V. V.; Merzlyakov, D. A.; Sobolev, V. V. Optical Properties and Electronic Structure of CaO. *Journal of Applied Spectroscopy* **2016**, *83*, 567–572.

- (45) Kumar, R.; Sharma, B. K.; Sharma, G. Electronic Structure and Momentum Density of BaO and BaS. *Advances in Condensed Matter Physics* **2013**, *2013*, 1–6.
- (46) xi Sun, R.; yu Liu, T.; li Wu, K.; yu Shi, C.; mei Song, J. First-principles study of electronic structure and magnetism in SrO crystal contained cation defects. *Journal of Magnetism and Magnetic Materials* **2021**, *522*, 167524.
- (47) Tsuchiya, T.; Kawamura, K. Systematics of elasticity: Ab initio study in B1-type alkaline earth oxides. *The Journal of Chemical Physics* **2001**, *114*, 10086–10093.
- (48) Guo, Y.-D.; Cheng, X.-L.; Zhou, L.-P.; Liu, Z.-J.; Yang, X.-D. First-principles calculation of elastic and thermodynamic properties of MgO and SrO under high pressure. *Physica B: Condensed Matter* **2006**, *373*, 334–340.
- (49) Pandey, V.; Gupta, S.; Rathi, S.; Goyal, S. Elastic properties of alkaline earth oxides under high pressure. *Phase Transitions* **2010**, *83*, 1059–1071.
- (50) Singh, S.; Singh, D.; Singh, N.; Shukla, M. Study of elastic properties of prototype solids under high pressure. *Computational Condensed Matter* **2022**, *30*, e00626.
- (51) Kumar, P.; Rajput, K.; Roy, D. R. Structural, electronic, vibrational, mechanical and thermoelectric properties of 2D and bulk BaX (X=O, S, Se and Te) series under DFT and BTE framework. *Physica E: Low-dimensional Systems and Nanostructures* **2021**, *127*, 114523.
- (52) Lukačević, I. High-pressure lattice dynamics and thermodynamics in BaO. *physica status solidi (b)* **2011**, *248*, 1405–1411.
- (53) Uludođan, M.; ÇađIn, T.; Strachan, A.; III, W. A. G. *Journal of Computer-Aided Materials Design* **2001**, *8*, 193–202.
- (54) Amorim, R. G.; Veríssimo-Alves, M.; Rino, J. P. Energetics of phase transitions in

- BaO through DFT calculations with norm-conserving pseudopotentials: LDA vs. GGA results. *Computational Materials Science* **2006**, *37*, 349–354.
- (55) Jog, K. N.; Singh, R. K.; Sanyal, S. P. Phase transition and high-pressure behavior of divalent metal oxides. *Physical Review B* **1985**, *31*, 6047–6057.
- (56) Wu, E. J. Applications of lattice dynamics theory: calculating vibrational entropy in alloys and dielectric losses in ceramics. Ph.D. thesis, Massachusetts Institute of Technology, 2002.
- (57) Musari, A. A.; Orukombo, S. A. Theoretical study of phonon dispersion, elastic, mechanical and thermodynamic properties of barium chalcogenides. *International Journal of Modern Physics B* **2018**, *32*, 1850092.
- (58) Chang, S.; Tompson, C.; Gürmen, E.; Muhlestein, L. Lattice dynamics of BaO. *Journal of Physics and Chemistry of Solids* **1975**, *36*, 769–773.
- (59) Kresse, G.; Furthmüller, J. Efficient iterative schemes for ab initio total-energy calculations using a plane-wave basis set. *Physical Review B* **1996**, *54*, 11169–11186.
- (60) Togo, A.; Tanaka, I. First principles phonon calculations in materials science. *Scripta Materialia* **2015**, *108*, 1–5.
- (61) Clark, S. J.; Segall, M. D.; Pickard, C. J.; Hasnip, P. J.; Probert, M. I. J.; Refson, K.; Payne, M. C. First principles methods using CASTEP. *Zeitschrift für Kristallographie - Crystalline Materials* **2005**, *220*, 567–570.
- (62) Momma, K.; Izumi, F. VESTA: a three-dimensional visualization system for electronic and structural analysis. *Journal of Applied Crystallography* **2008**, *41*, 653–658.
- (63) Hellman, O.; Abrikosov, I. A.; Simak, S. I. Lattice Dynamics of Anharmonic Solids from First Principles. *Phys. Rev. B* **2011**, *84*, 180301.

- (64) Liu, L. A Dense Modification of BaO and Its Crystal Structure. *Journal of Applied Physics* **1971**, *42*, 3702–3704.
- (65) Catti, M. Ab initio predicted metastable TII-like phase in the B1to B2 high-pressure transition of CaO. *Physical Review B* **2003**, *68*.
- (66) Birch, F. Finite Elastic Strain of Cubic Crystals. *Phys. Rev.* **1947**, *71*, 809–824.
- (67) Cinthia, A. J.; Priyanga, G. S.; Rajeswarapalanichamy, R.; Iyakutti, K. Structural, electronic and mechanical properties of alkaline earth metal oxides MO (M=Be, Mg, Ca, Sr, Ba). *Journal of Physics and Chemistry of Solids* **2015**, *79*, 23–42.
- (68) Mouhat, F.; Coudert, F. m. c.-X. Necessary and sufficient elastic stability conditions in various crystal systems. *Phys. Rev. B* **2014**, *90*, 224104.
- (69) Rakesh Roshan, S. C.; Yedukondalu, N.; Muthaiah, R.; Lavanya, K.; Anees, P.; Kumar, R. R.; Rao, T. V.; Ehm, L.; Parise, J. B. Anomalous Lattice Thermal Conductivity in Rocksalt IIA–VIA Compounds. *ACS Applied Energy Materials* **2022**, *5*, 882–896.
- (70) Efthimiopoulos, I.; Kunc, K.; Karmakar, S.; Syassen, K.; Hanfland, M.; Vajenine, G. Structural transformation and vibrational properties of BaO₂ at high pressures. *Physical Review B* **2010**, *82*.
- (71) Yamaoka, S.; Shimomura, O.; Nakazawa, H.; Fukunaga, O. Pressure-induced phase transformation in BaS. *Solid State Communications* **1980**, *33*, 87–89.
- (72) Lin, G. Q.; Gong, H.; Wu, P. Electronic properties of barium chalcogenides from first-principles calculations: Tailoring wide-band-gap II–VI semiconductors. *Physical Review B* **2005**, *71*.
- (73) Vetter, V.; Bartels, R. BaO single crystal elastic constants and their temperature dependence. *Journal of Physics and Chemistry of Solids* **1973**, *34*, 1448–1449.

- (74) Chang, Z.; Graham, E. Elastic properties of oxides in the NaCl-structure. *Journal of Physics and Chemistry of Solids* **1977**, *38*, 1355–1362.
- (75) Ghebouli, M.; Ghebouli, B.; Bouhemadou, A.; Fatmi, M.; Bouamama, K. Structural, electronic, optical and thermodynamic properties of $\text{Sr}_x\text{Ca}_{1-x}\text{O}$, $\text{Ba}_x\text{Sr}_{1-x}\text{O}$ and $\text{Ba}_x\text{Ca}_{1-x}\text{O}$ alloys. *Journal of Alloys and Compounds* **2011**, *509*, 1440–1447.
- (76) Cortona, P.; Monteleone, A. V. Ab initio calculations of cohesive and structural properties of the alkali-earth oxides. *Journal of Physics: Condensed Matter* **1996**, *8*, 8983–8994.

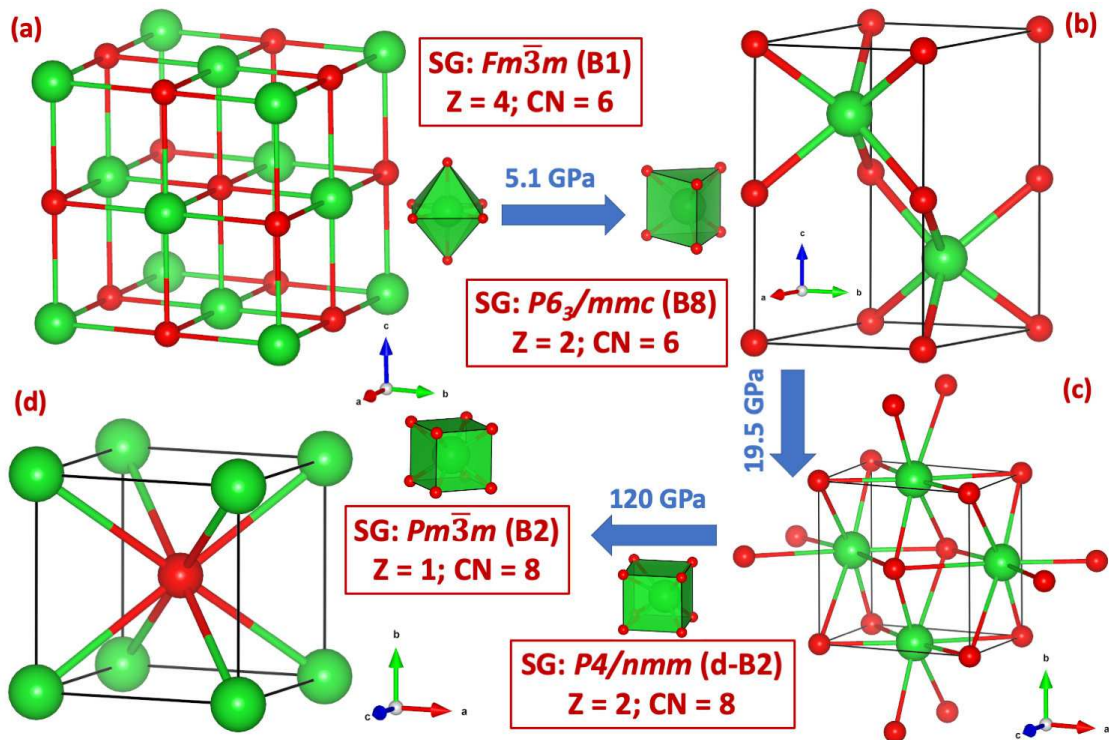


Figure 1: Crystal structure of (a) ambient rocksalt NaCl-type (B1) and high pressure (b) NiAs-type (B8), (c) PH₄-type distorted CsCl-type (d-B2) and (d) CsCl-type (B2) phases of BaO. Where SG and CN denote space group and coordination number, respectively. Green and red color balls represent Ba and O atoms, respectively.

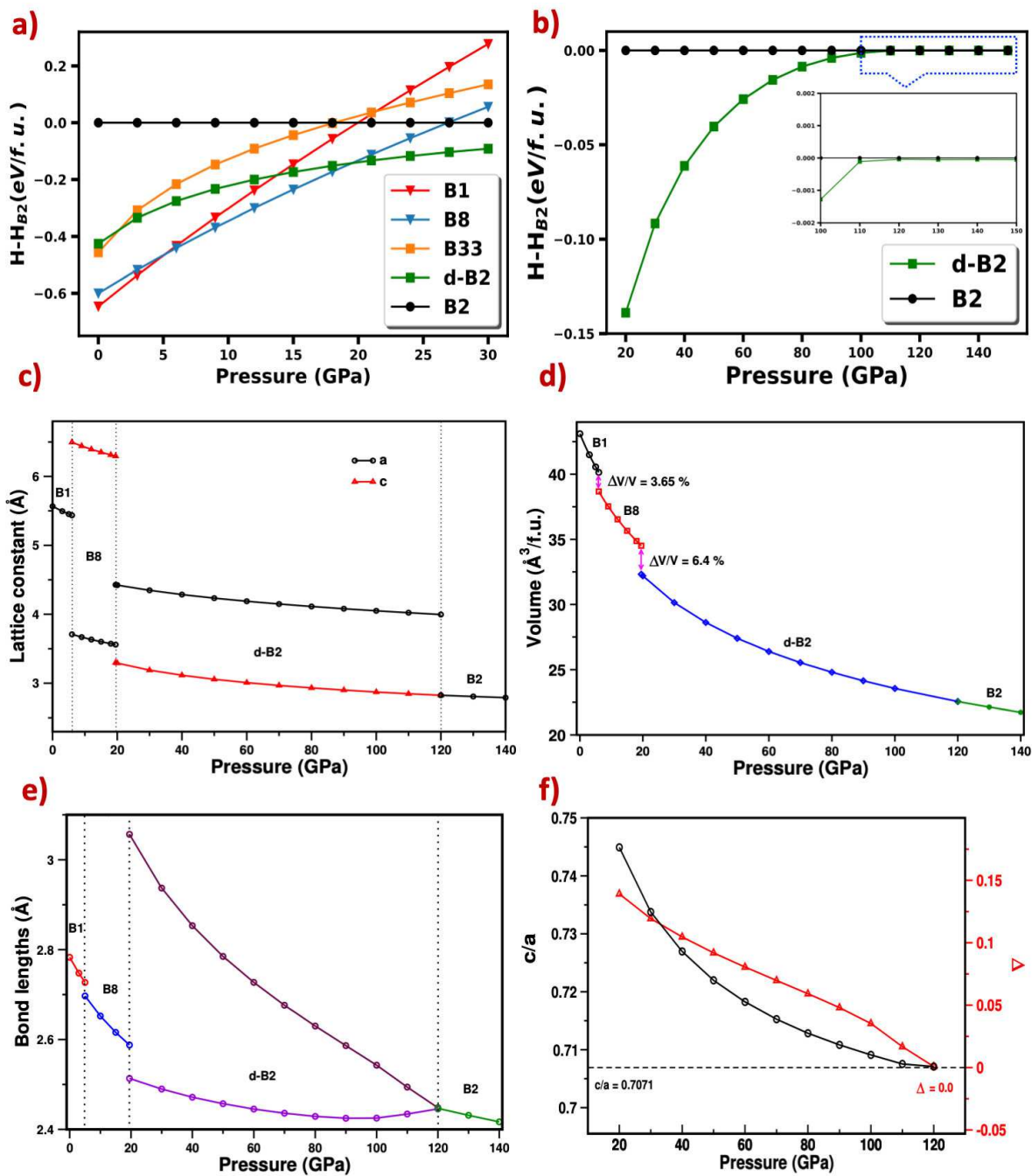


Figure 2: Calculated (a,b) relative enthalpy difference of B1, B8, B33, d-B2 phases w.r.t B2 phase, (c) lattice constants, (d) volume, (e) bond lengths for B1, B8, DB2 and B2 phases as a function of pressure and (f) variation of c/a ratio and Δ with pressure for d-B2 phase.

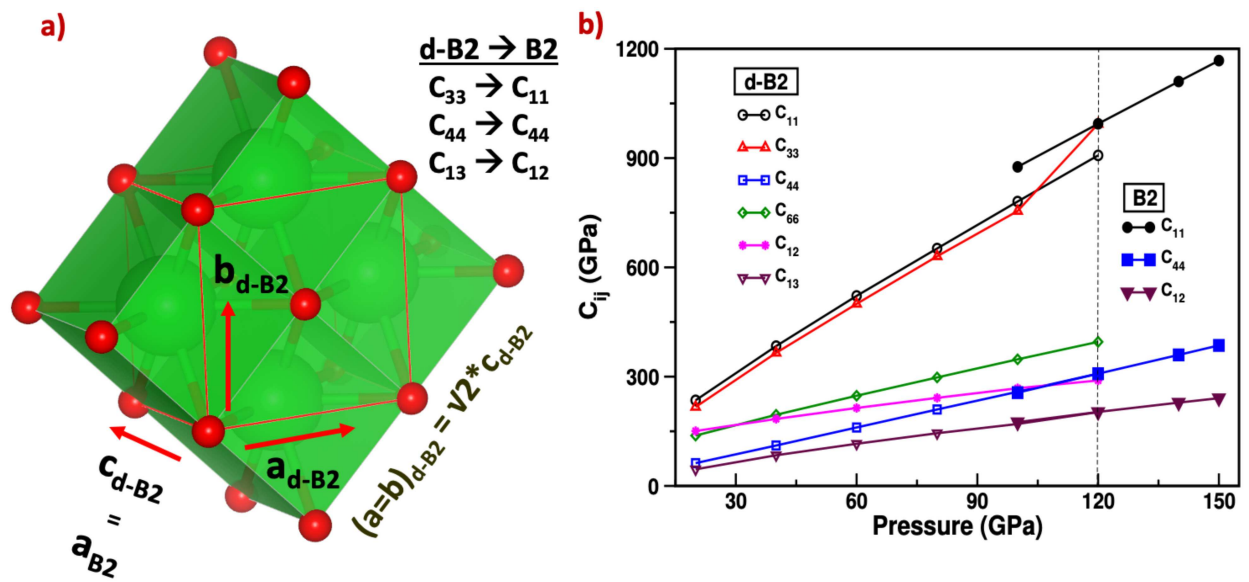


Figure 3: (a) Lattice transformation from d-B2 to B2 and (b) calculated elastic constants of d-B2 and B2 phases of BaO as a function of pressure.

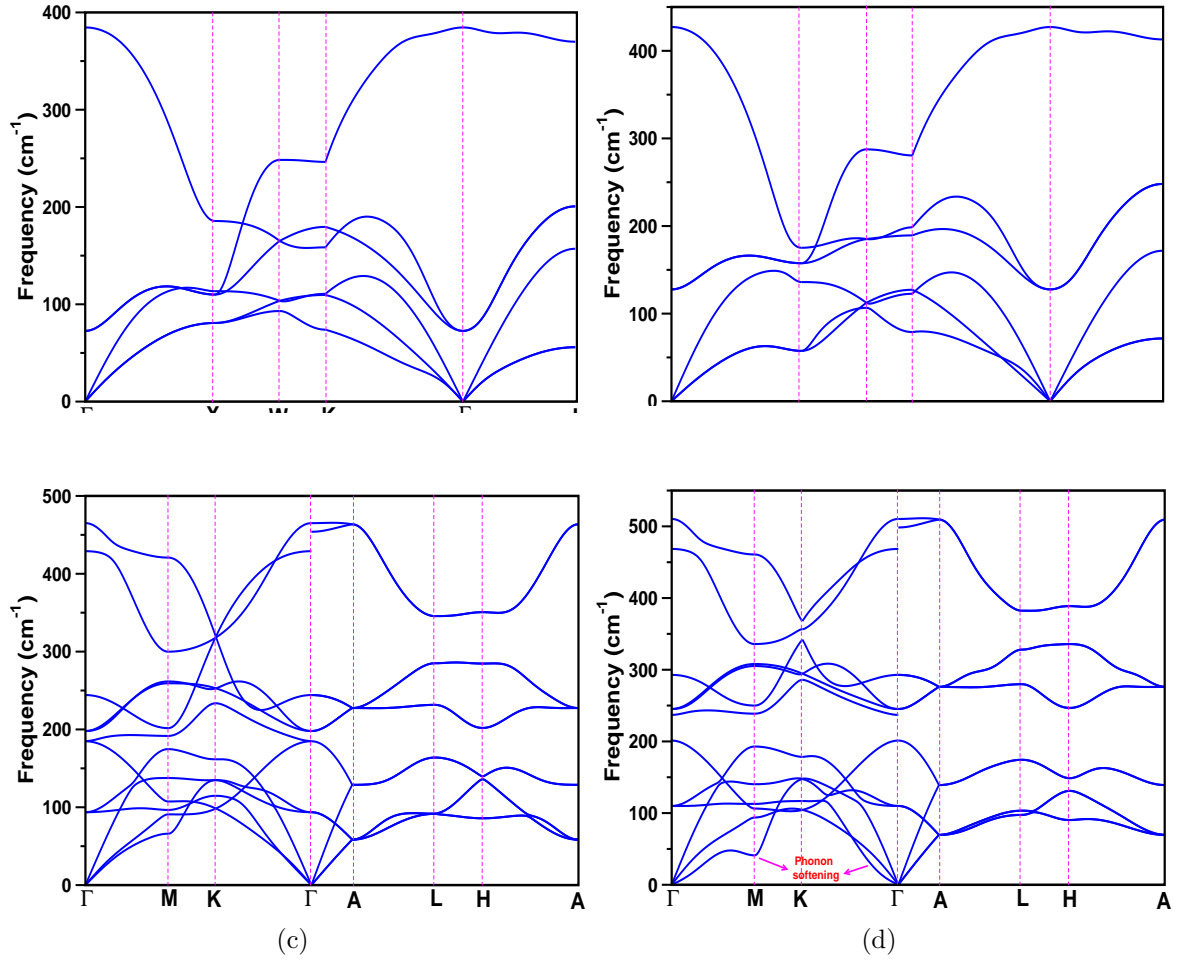


Figure 4: Calculated phonon dispersion curves of (a, b) B1 phase at (a) 0, (b) 9 GPa and for (c, d) B8 phase at (c) 9 GPa, (d) 20 GPa. Phonon softening is observed along X-direction for B1 phase and for B8 phase at high pressure (20 GPa) along M and K- Γ directions, which destabilize the B1 and B8 phases upon further compression.

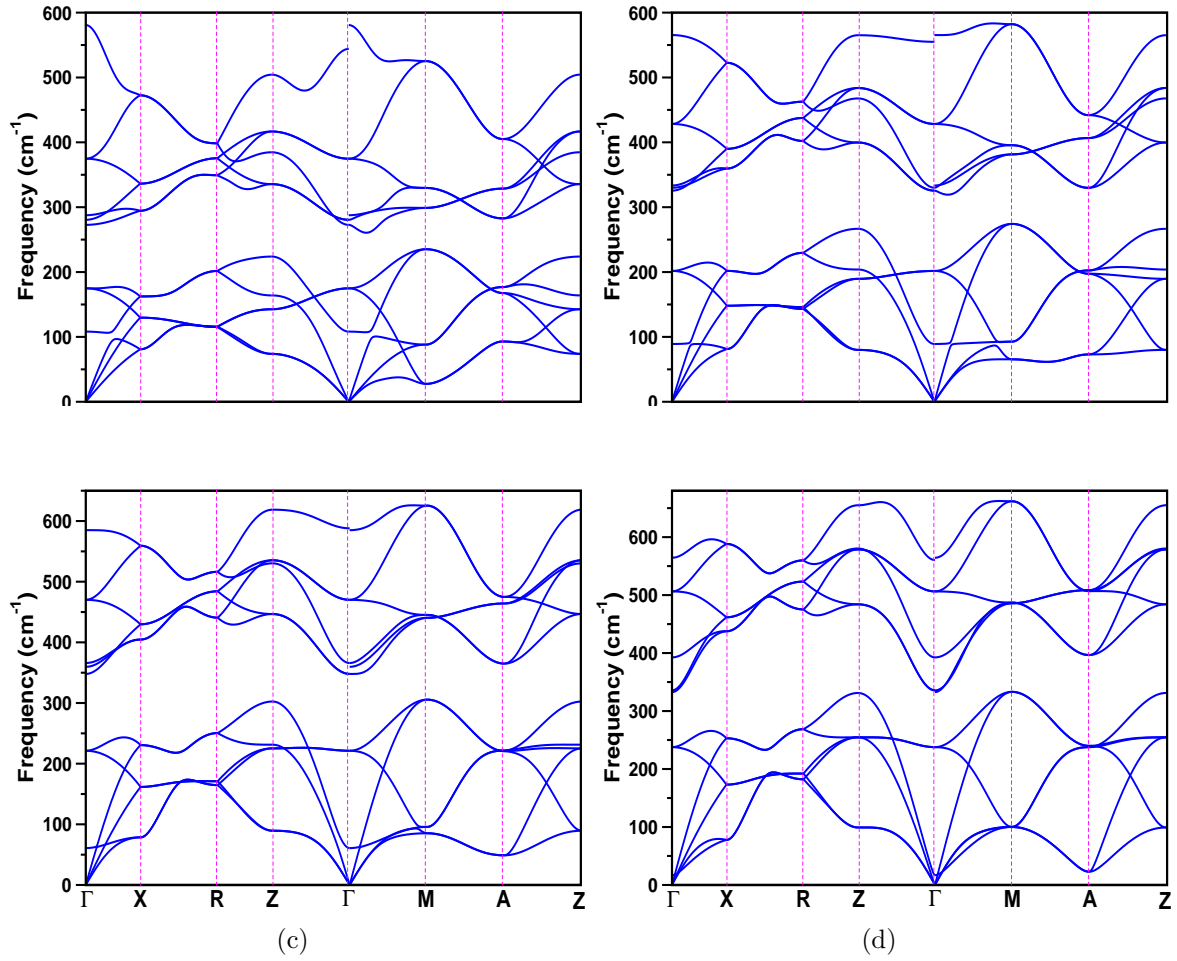


Figure 5: Calculated phonon dispersion curves for d-B2 phase at (a) 30, (b) 60, (c) 90 and (d) 120 GPa. Optical phonon softening along Z- Γ direction and acoustic phonon softening along A-direction are observed with pressure and it is predominant above 90 GPa.

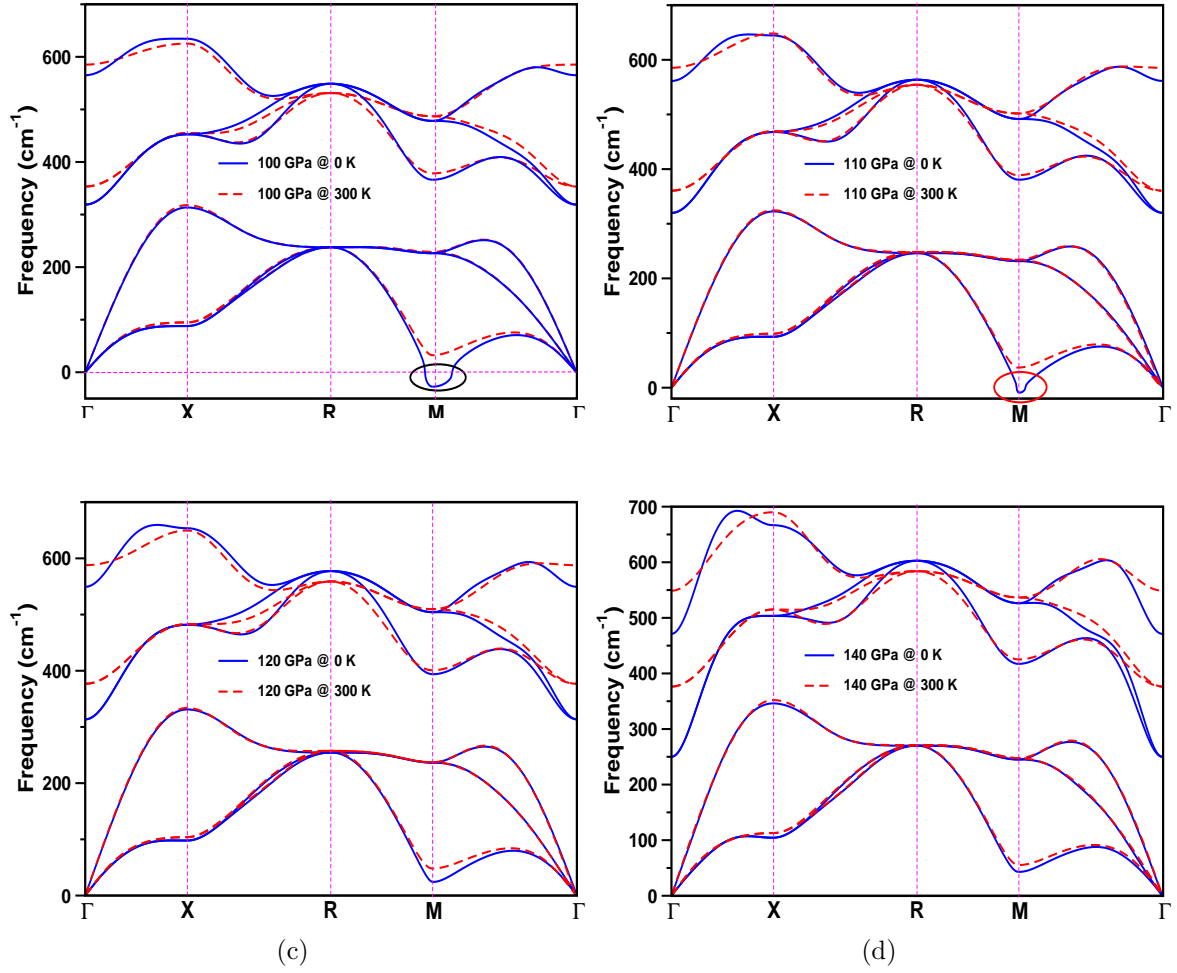


Figure 6: Calculated phonon dispersion curves for B2 phase at high pressures (a) 100 GPa, (b) 110 GPa (c) 120 GPa and (d) 140 GPa at 0K as well as at 300 K. B2 phase is dynamically stable including anharmonic effects at 100 and 110 GPa at 300 K but it is dynamically unstable within the harmonic approximation at 0 K.

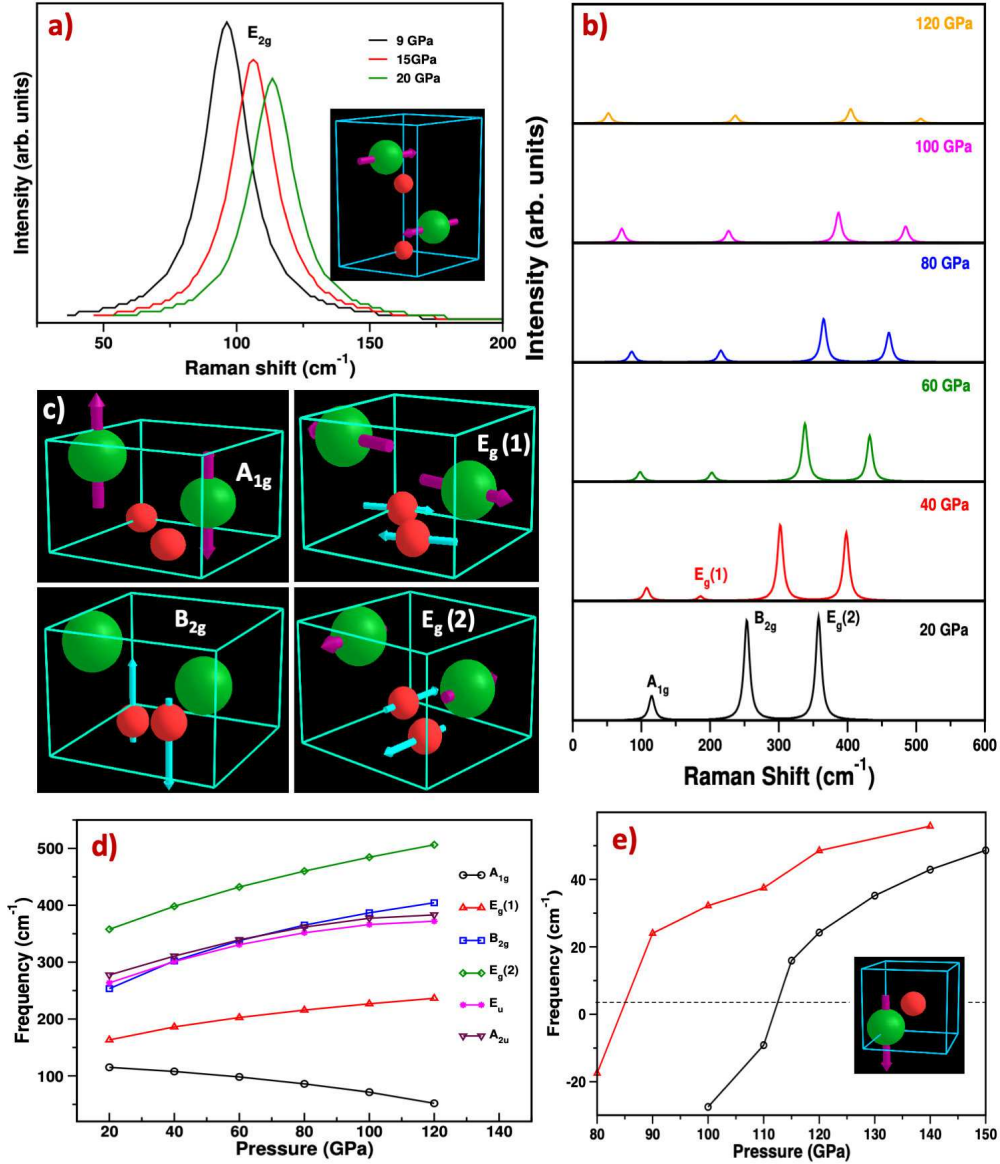


Figure 7: Calculated Raman spectra of (a) B8 and (b) d-B2 phase as a function of pressure. Eigen vectors of Raman active modes are presented for (a) B8 and (c) d-B2 phases of BaO. Pressure evolution of (d) Raman and IR active modes of d-B2 phase and (e) Transverse acoustic mode of B2 phase along M-high symmetry direction without and with inclusion of anharmonic effects.

Table 1: Calculated equilibrium lattice constants (a, c in Å) of BaO at ambient and high pressure and are compared with the available X-ray diffraction data and other first principles calculations.

Phase	Pressure	This work	Expt.	Others
B1	0	a=5.533	5.520 ^a	5.562 ^b , 5.454 ^b , 5.614 ^c , 5.604 ^d , 5.552 ^e , 5.462 ^f
B8	13.9	a= 3.612,c= 6.365	a= 3.617,c= 6.349 ^g	-
d-B2	60.5	a= 4.187,c= 3.007	a= 4.1,c= 2.998 ^g	-
B2	130	a=2.8	-	-

^aRef. ⁷¹ ^bRef. ⁷² ^cRef. ⁵¹ ^dRef. ⁶⁷ ^eRef. ⁴⁷ ^f Ref. ¹⁹ ^g Ref. ³¹

Table 2: Calculated phase transition pressure (P_t , in GPa) and volume collapse (VC in %) of BaO and are compared with the available experimental data and other first principles calculations.

Parameter	Transition	This Work	Expt.	Others
P_t	B1 \rightarrow B8	5.1	9.2 ^a , 10 ^b	5 ^c , 4.3 ^d
	B8 \rightarrow d-B2	19.5	18 ^a , 18.8 ^b	13 ^c , 23.2 ^d
VC	B1 \rightarrow B8	3.65	5 ^a	3.6 ^e , 1.5 ^f
	B8 \rightarrow d-B2	6.4	7 ^a	8.7 ^e

^a Ref. ³⁰ ^b Ref. ³¹ ^c Ref. ¹⁷ ^d Ref. ⁵⁴ ^eRef. ⁵³ ^fRef. ⁵²

Table 3: Calculated equilibrium bulk modulus (B_0) and its pressure derivative (B_0') of ambient and high pressure phases of BaO and are compared with the available experimental data and previous first principles calculations.

Phase	Pressure range	B_0 (B_0')	Expt.	Others
B1	0-9	71.4 (4.35)	69 ^a , 66.2 ^b , 61 ^c 74.1 ^b , 74.06 ^h (5.07 ^h)	68.912 ^d (4.09 ^d), 73 ^e (4.3 ^e), 71.22 ^f (4.52 ^f), 75.7 ^g , 62.75 ⁱ , 71.72 ^j , 73 ^k
B8	6-30	68.6(4.32)	-	68.04 ^f (4.19 ^f), 72.7 ^g
d-B2	20-120	51.3 (4.67)	33.2 ^b (6.02 ^b),	27.13 ^f , 41.8 ^g
B2	70-150	90.6 (4.15)	-	74.69 ^f (4.07 ^f), 72.57 ^d (3.7 ^d), 86 ^l , 59.1 ^g

^a Ref. ³⁰ ^b Ref. ³¹ ^c Ref. ⁷³ ^d Ref. ¹⁹ ^eRef. ⁴⁷ ^fRef. ⁵³ ^g Ref. ⁵⁴ ^hRef. ⁷⁴ ⁱRef. ⁴⁹ ^jRef. ⁷⁵ ^k Ref. ⁵⁵ ^l Ref. ⁷⁶

Supporting Information

Lattice instability, anharmonicity and Raman spectra of BaO under high pressure: A first principles study

K. Lavanya,^{†,‡} N. Yedukondalu,^{*,¶} S. C. Rakesh Roshan,^{§,||} Shweta D. Dabhi,[⊥]
Suresh Sripada,[#] M.Sainath,^{*,@} Lars Ehm,[¶] and John B. Parise[¶]

[†]*Jawaharlal Nehru Technological University (JNTU), Hyderabad, 500085, Telangana, India.*

[‡]*Telangana Social Welfare Residential Degree College for Women (TSWRDC-W), Nizamabad, 503002, Telangana, India.*

[¶]*Department of Geosciences, State University of New York, Stony Brook, New York 11794-2100, USA*

[§]*Rajiv Gandhi University of Knowledge Technologies, Basar, Telangana-504107, India*

^{||}*Department of Physics, National Institute of Technology-Warangal, Telangana, India*

[⊥]*Department of Physical Sciences, P D Patel Institute of Applied Sciences, Charotar University of Science and Technology, CHARUSAT Campus, Changa, 388421, Gujarat, India*

[#]*Department of Physics, JNTUHCEJ, 505501 Karimnagar, Telangana, India*

[@]*Department of Physics, IcfaiTech, IFHE, Hyderabad 501203, Telangana, India.*

E-mail: nykondalu@gmail.com; sai1968@gmail.com

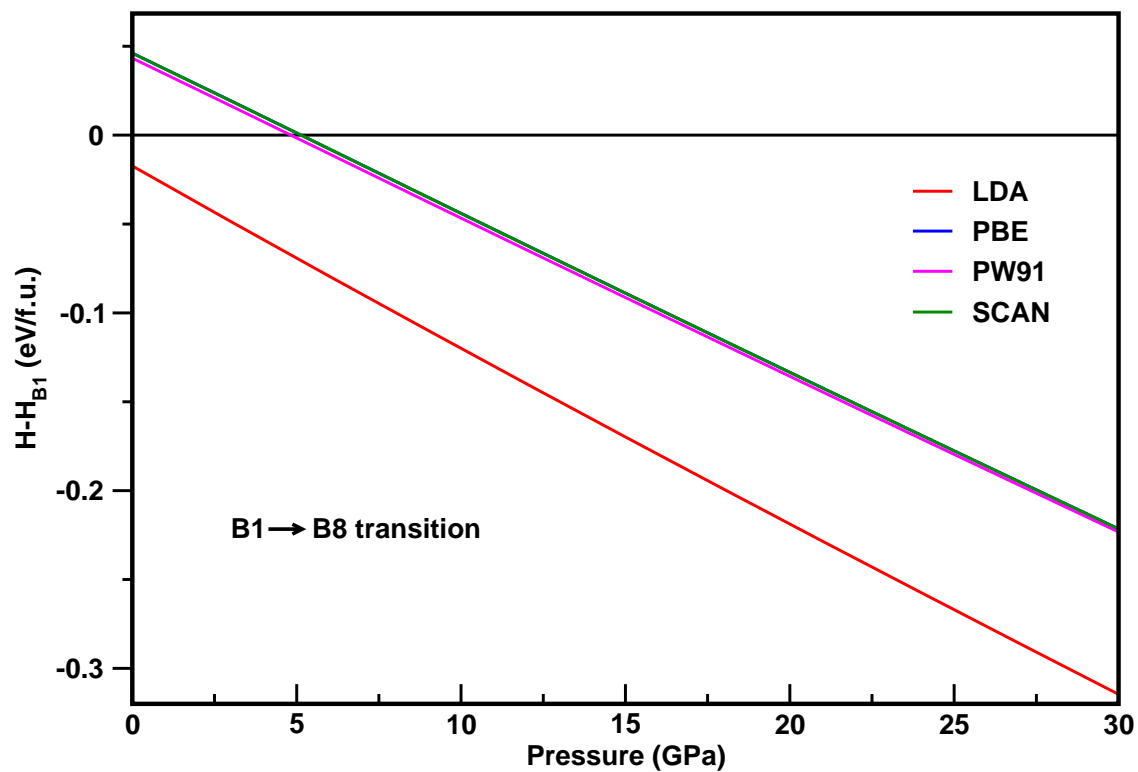


Figure S1: Calculated relative enthalpy difference of B8 phase w.r.t B1 phase for BaO using various functionals such as LDA, PBE, PW91 and SCAN.

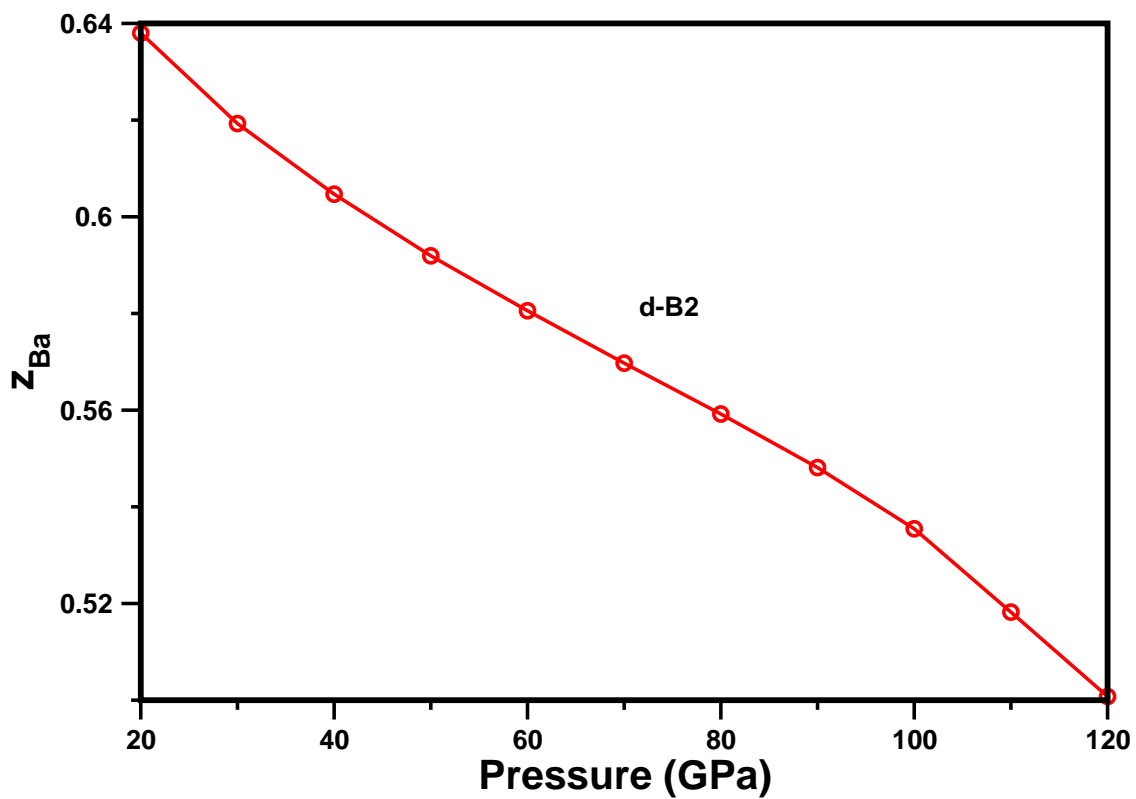


Figure S2: Displacive nature of z_{Ba} as a function of pressure for d-B2 phase in the pressure range of 20-120 GPa.

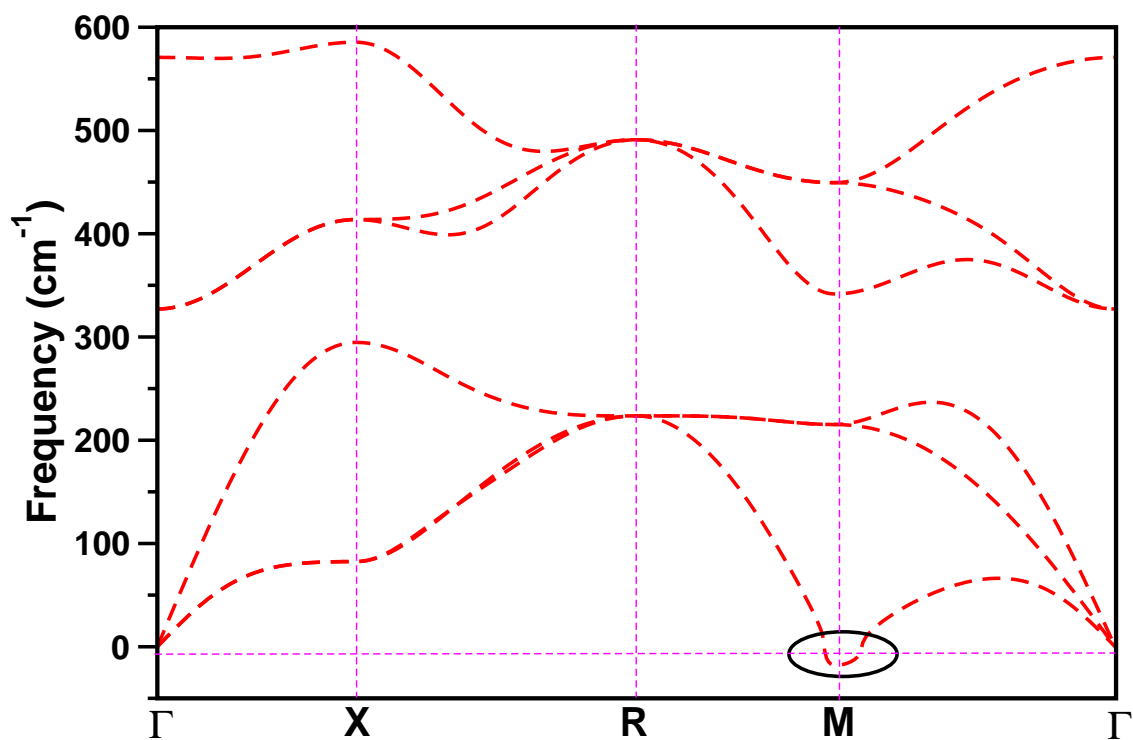


Figure S3: Calculated phonon dispersion curves of B2 phase at 80 GPa and 300 K using ab-initio molecular dynamics (AIMD) and temperature dependent effective potential (TDEP).